Characterization

A field-emission scanning electron microscope (FESEM, HITACHI SU-8000; Operating Voltage 5 kV) was used initially to characterize the morphology of the mesoporous iridium oxide nanosheets. The IrO_x-150 for SEM was prepared by depositing a drop of a diluted colloidal suspension of the as-prepared nanosheets on a clean silicon (Si) substrate. Then the Si substrate and sample were annealed at 150 °C for 1 h in air prior to SEM observation. High-resolution transmission electron microscopy (HRTEM, JEOL JEM-2100F) images were collected at an operation voltage of 200 kV. The amorphous mesoporous IrO_x-150 samples for TEM and HRTEM measurements were prepared by depositing a drop of a diluted solution of the as-prepared nanosheets on a TEM grid, then TEM grid and sample were heated together at 150°C in air for 1 hour. Powder X-ray diffraction (XRD) patterns were collected with a Smart lab X-ray diffractometer (RIGAKU) at a scanning rate of 1 ° min^{-1} using a Cu Kα radiation source (40 kV, 30 mA). Low-angle XRD measurements (Rigaku NANO-Viewer) were used to evaluate the pore-to-pore distance. X-ray photoelectron spectroscopy (XPS) was performed on a JPS-9010TR (JEOL) instrument with an Mg Kα X-ray source. All the binding energies were calibrated using the C-*1s* binding energy peak (284.5 eV) as a reference. Inductively coupled plasma optical emission spectrometer (ICP-OES) was performed on a Hitachi model SPS3520UV-DD. Nitrogen adsorption-desorption isotherms were acquired by using a BELSORP-mini (BEL, Japan) at 77 K and surface area was estimated using the Multipoint Brunauer-Emmett-Teller (BET) method. Thermal gravimetric (TG) analysis was obtained with a Hitachi HT-Seiko Instrument Exter 6300 TG/DTA. Fourier transform infrared spectroscopic (FTIR) measurements were recorded on a thermoscientific Nicolet 4700 using KBr pellets. The low-angle XRD measurement used a Cu Kα radiation (40 kV, 30 mA) source with a camera length at 700 mm. The spectra of Ir-L_{III} edge in mesoporous IrO_x-150 was measured at room temperature by using BL-01C1 at the National Synchrotron Radiation Research Center (NSRRC, Hsinchu, Taiwan), where the electron storage ring was operated at 1.5 GeV with a beam current of 300 mA.

Electrochemical measurement

3 mg of the as-prepared nanosheets were dispersed in 5 mL ethanol/acetone mixture by ultrasonic treatment for 2 hours. Then 6 mg of the ethanol suspension containing Vulcan XC-72 carbon (1 mg mL^{-1}) (Premetek Co.) was mixed with the above nanosheet solution and then vortexed at 900 rpm for 15 hours. The carbon supported samples were collected by centrifugation (12,000 rpm for 20 minutes) and then washed with ethanol to remove impurities and calcinated at 150 °C and 400 °C in air for 1 h to obtain the carbon supported amorphous mesoporous IrO_x nanosheets and crystallized IrO_2 nanosheets, respectively. The carbon-supported mesoporous iridium oxide nanosheets samples and commercial IrO_2 were dispersed in a mixture containing water, acetone, ethanol and Nafion (5 %) and then sonicated for 1 hour to form a homogeneous catalyst ink. Catalyst-supported electrodes were prepared with a glassy carbon electrode (GCE; diameter = 3 mm). The GCE was carefully polished, washed and dried in air at room temperature. Then the catalyst suspension (6 μL) was deposited on its

surface. The GCE was used as the working electrode after the solvent had evaporated. An inductively coupled plasma optical emission spectrometer (ICP-OES) was used to measure the concentration of iridium oxide in the samples. The Ir concentrations of the mesoporous IrO_x-150 and mesoporous IrO_2-400 samples were ~26 % and ~46 %, respectively. The loading amount of Ir on the glassy carbon (GC) electrode was ~7.8 μg for each electrocatalyst.

Electrochemical investigations were performed using an electrochemical workstation (BioLogic Science Instruments; VMP3) that measured cyclic voltammograms and steady-state linear-sweep voltammetry (LSV) measurements. The three-electrode cell consists of a reference electrode (saturated calomel electrode, SCE), a counter electrode (carbon rod) and a working electrode (GCE coated with catalyst). OER measurements were performed in a 0.5 M H_2SO_4 solution at a scan rate of 5 $mV \cdot s^{-1}$. All measured potentials are relative to a reversible hydrogen electrode (RHE) following the equation: $E_{RHE} = E_{SCE} + (0.241 + 0.059 \times pH)$. The ohmic potential drop (iR) losses that arise from the solution resistance were all corrected. Tafel plots of the overpotential versus the log(current density) were recorded with linear portions at low overpotentials fitted to the Tafel equation: $\eta = a + b \log j$, where η is the overpotential, b is the Tafel slope, j is the current density, and a is the exchange current density. The long-term durability of the catalysts was evaluated using chronopotentiometry in 0.5 M H_2SO_4 at a constant current density of 2.5 mA cm^{-2} over 12 h. The alkaline OER activity and stability of the samples were measured in 1 KOH at a constant current density of 10 mA cm^{-2} over 10 h. Cyclic voltammetry was carried out to probe the electrochemical double layer capacitance (C_{dl}) of three samples at non-Faradaic potentials between 1.14 and 1.24 V (*vs.* RHE in 0.5 M H_2SO_4) with sweep rates of 10, 20, 40, 60, 80, 100 mV s^{-1}. By plotting the difference of current density between the anodic and cathodic sweeps at 1.19 V *vs.* RHE in 0.5 M H_2SO_4 against the scan rate, a linear slope which is equivalent to twice the value of the C_{dl}, was obtained.

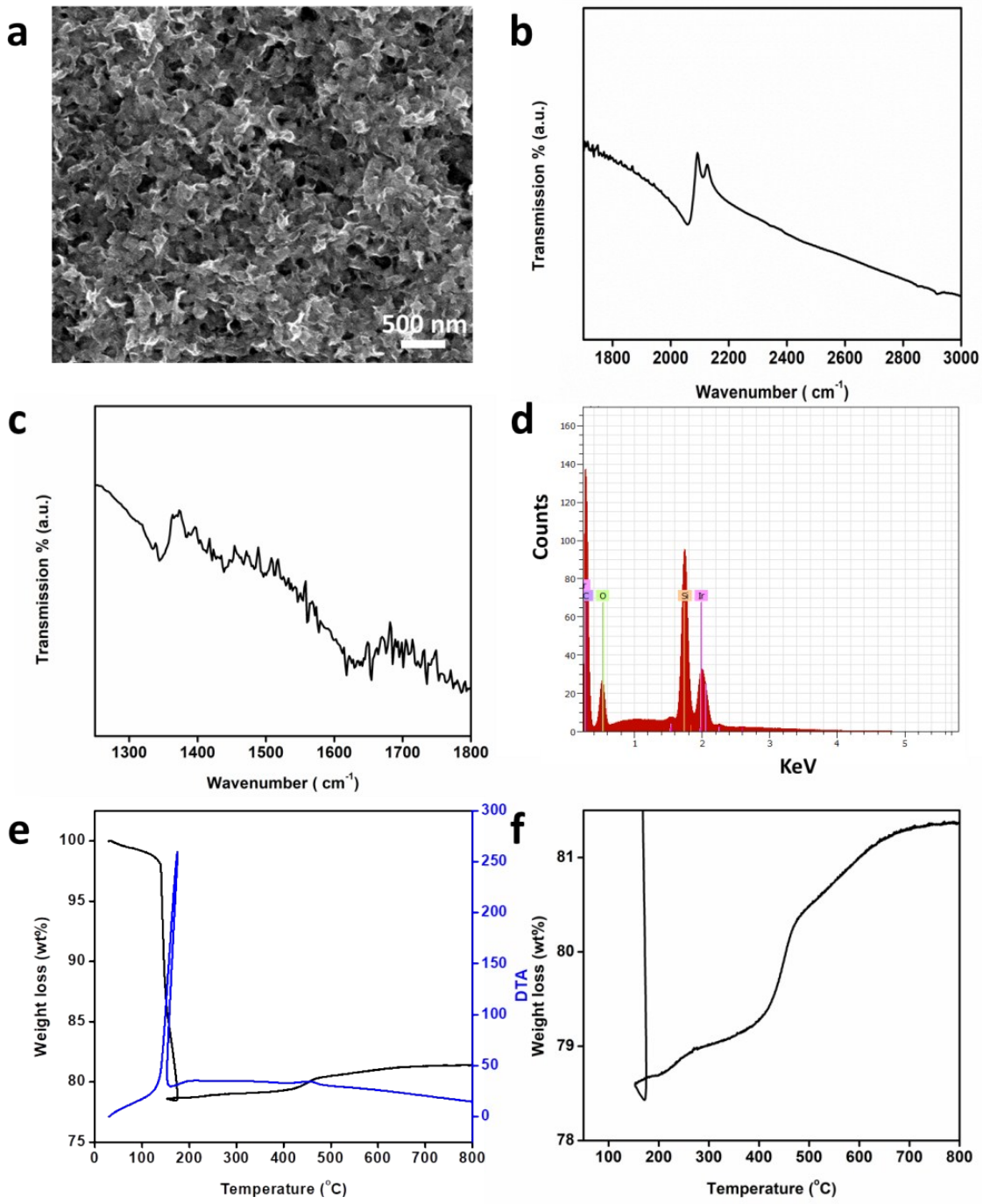

Figure S1 Analytical and structural characterization of the as-prepared mesoporous Ir nanosheets before calcination. (a) SEM image, (b) FT-IR spectrum, (c) enlarged FTIR spectrum (d) EDX, (e) TG/DTA curves and (f) an enlarged plot of the TG curves carried out in an air atmosphere.

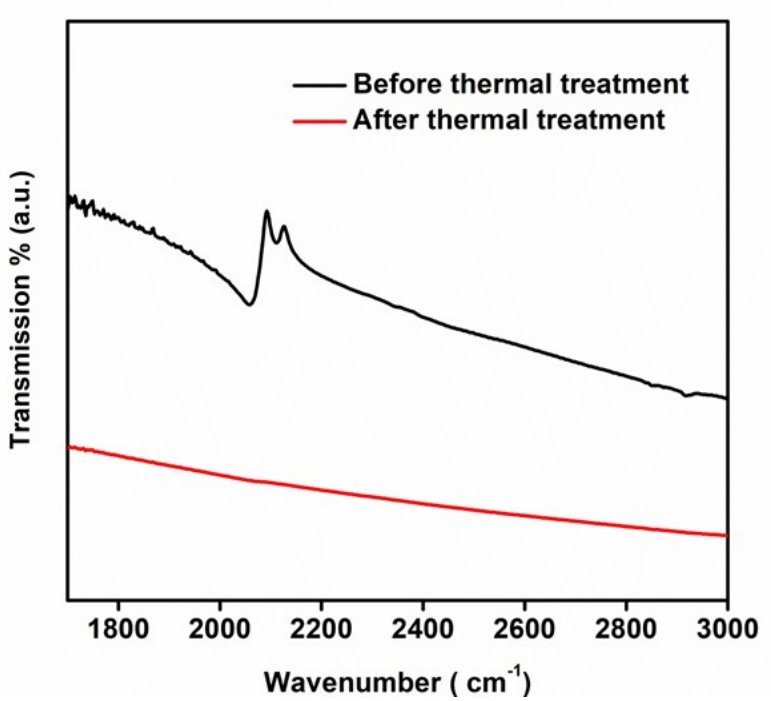

Figure S2 FTIR spectra of the as-prepared mesoporous Ir nanosheets before and after thermal treatment.

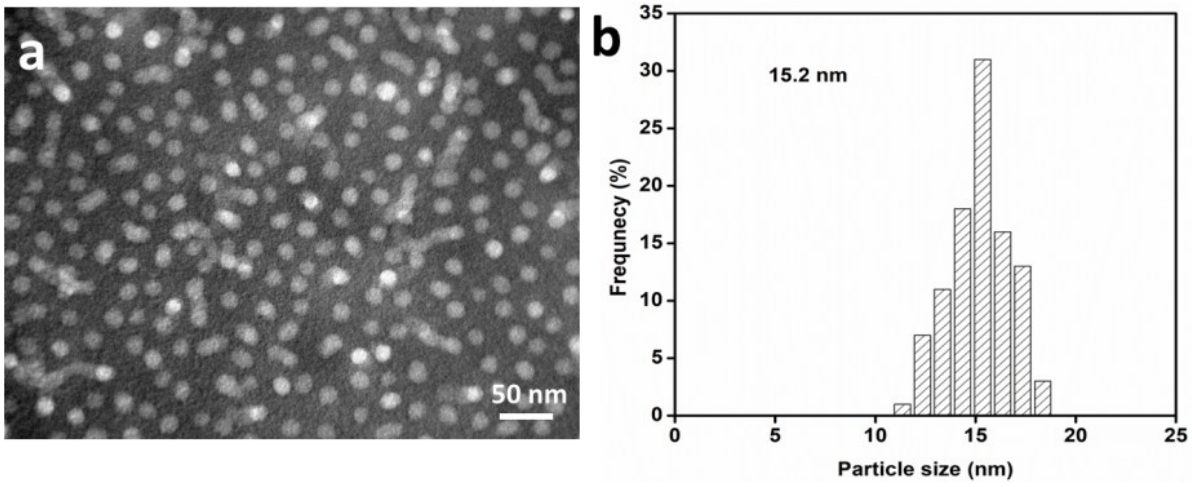

Figure S3 (a) TEM image and (b) particle size distribution histograms showing PEO-*b*-PS polymeric micelles obtained from DMF + PEO-*b*-PS + water + formic acid + $IrCl_3$. 1.0 wt% phosphotungstic acid was used to stain the TEM samples.

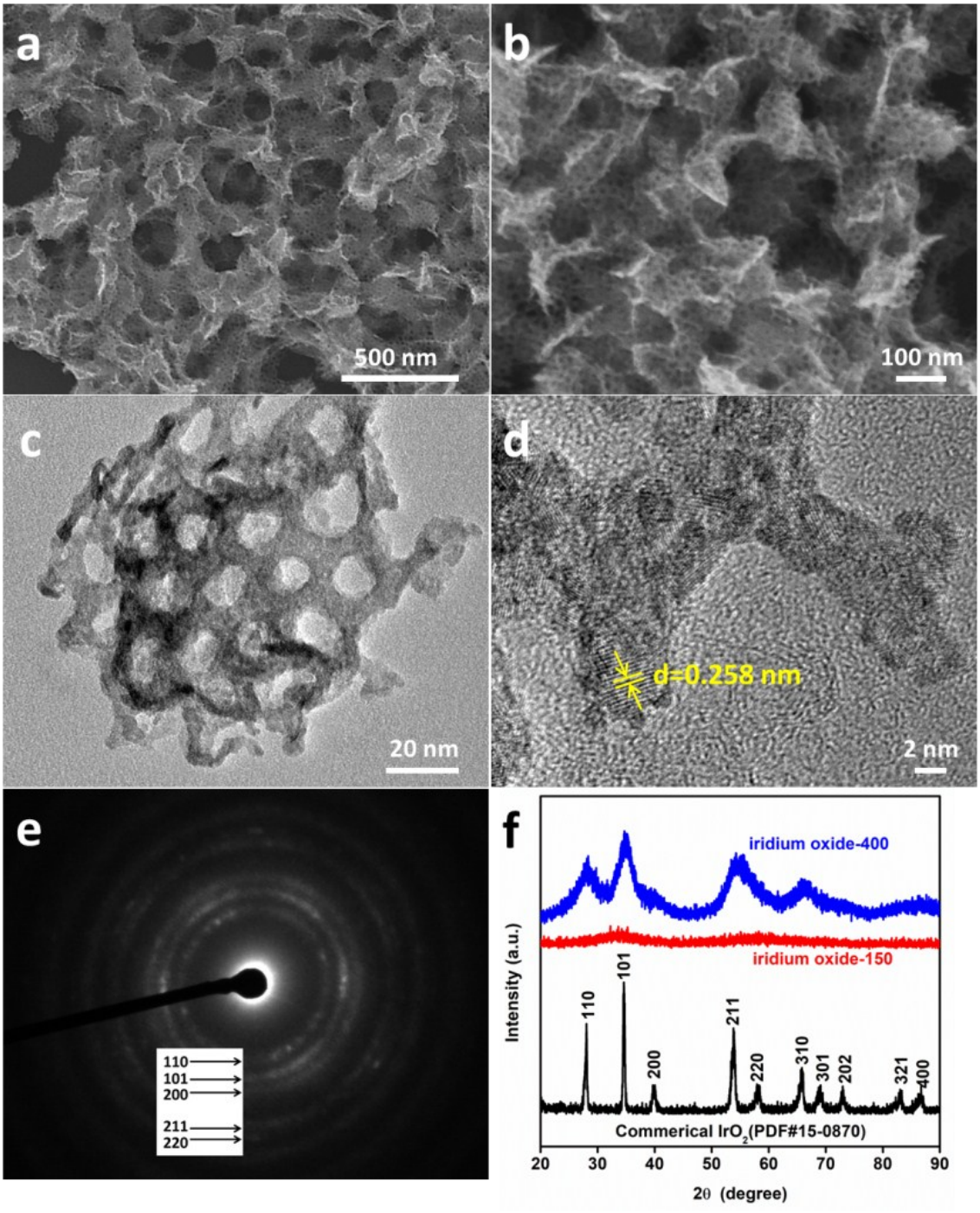

Figure S4 (a, b) SEM images, (c, d) TEM images, and (e) ED patterns of the crystallized mesoporous IrO_2-400 nanosheets obtained by annealing them at 400 ^oC for 1 h at air atmosphere. (f) Wide-angle XRD patterns of commercial IrO_2, amorphous mesoporous IrO_x-150, and crystallized mesoporous IrO_2-400 samples.

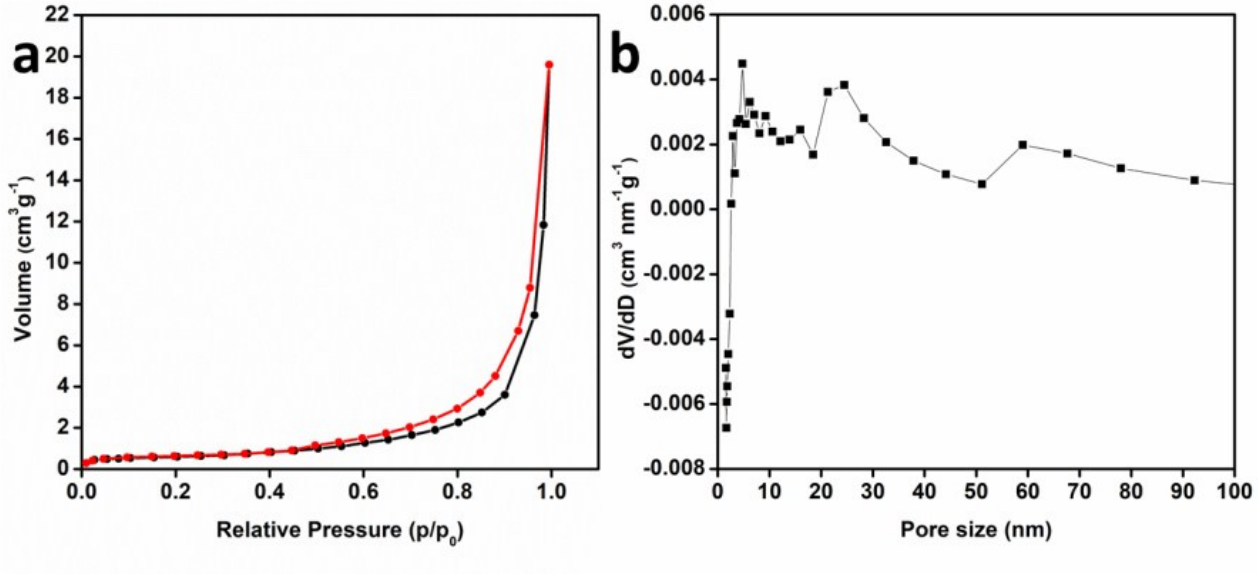

Figure S5 (a) N_2 adsorption-desorption isotherm of the commercial IrO_2. (b) BJH pore size distribution curve of the commercial IrO_2.

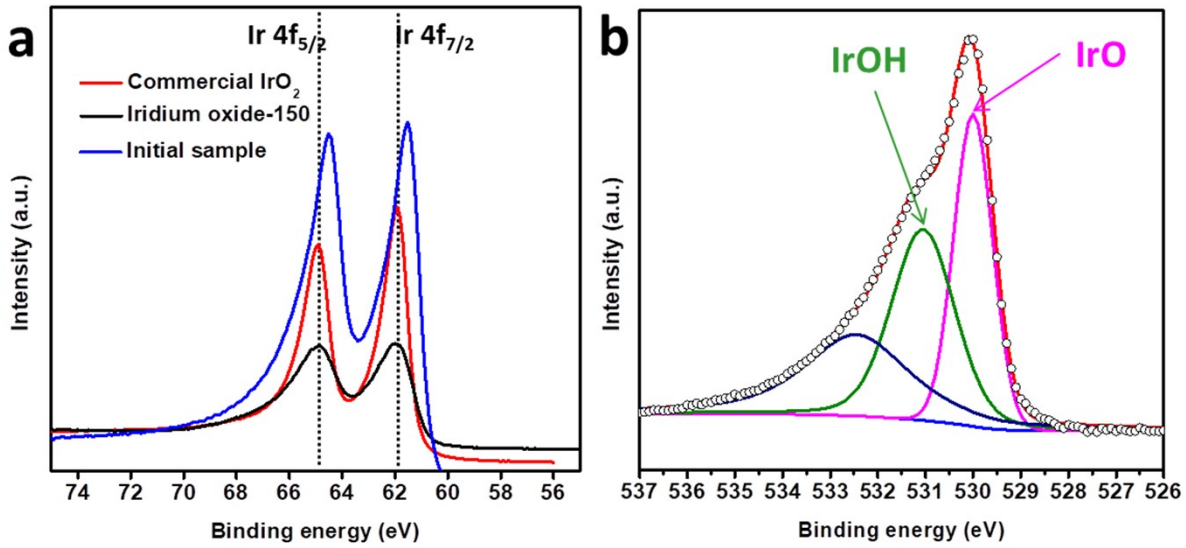

Figure S6 (a) XPS spectra of Ir *4f* peaks for the IrO_x-150 and commercial IrO_2 samples, and initial sample (*i.e.*, sample before heat treatment), (b) XPS spectra of O *1s* peak for the commercial IrO_2 sample. Another unmarked O 1s peak in Fig. S6b can be assigned to the presence of oxygen components from adventitious H_2O or carbon species.

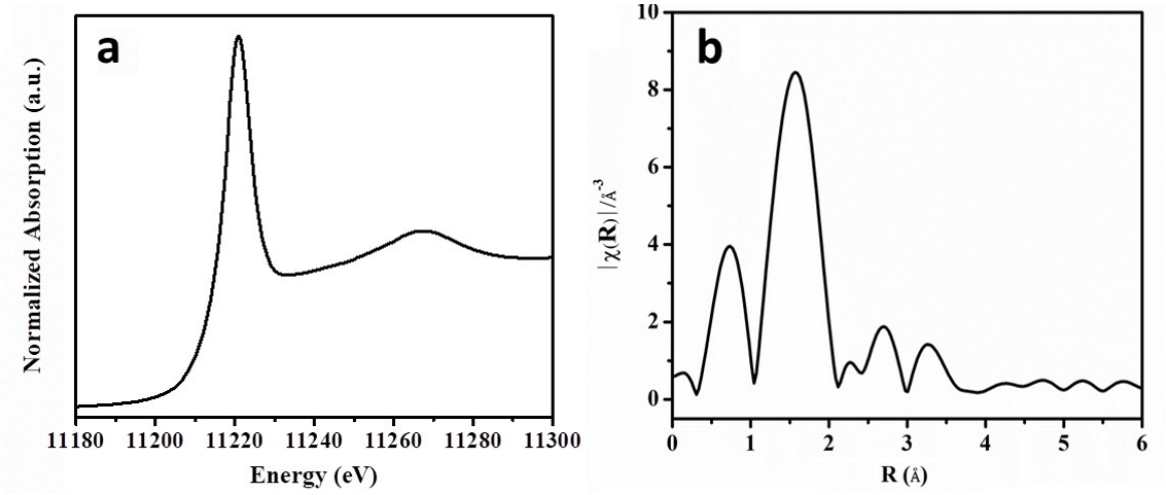

Figure S7 (a) The Ir L_3-edge XANES spectrum of IrO_x-150 sample and (b) the corresponding FT curves of the Ir L_3-edge EXAFS spectrum.

Table S1. EXAFS fitting parameters for the amorphous IrO_x-150 sample.

	R (Å)	N	ΔE (eV)	σ^2 (Å^2)
IrO_x-150	1.99(1)	5.6(0.3)	8.4(0.6)	0.0067(1)

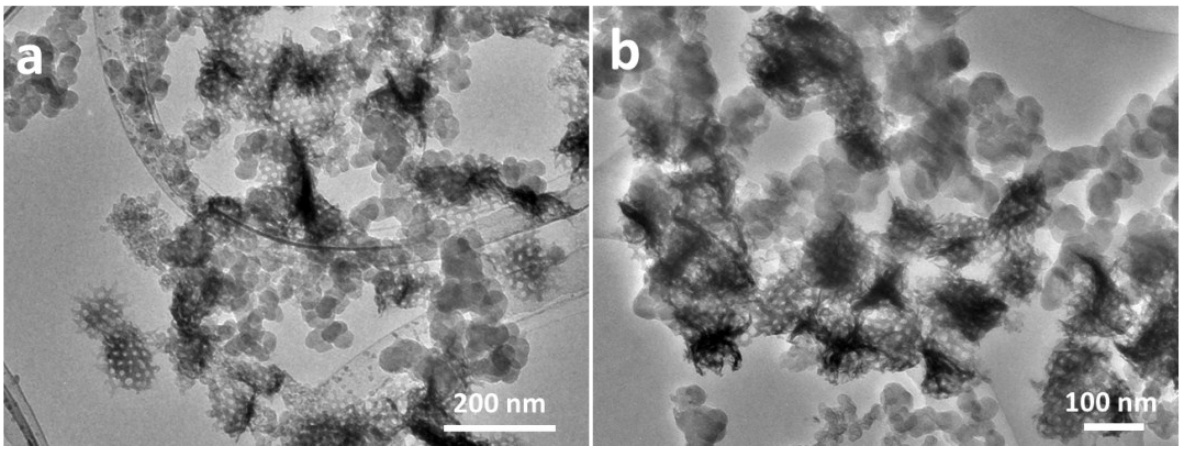

Figure S8 TEM images of (a) amorphous mesoporous IrO_x-150 and (b) mesoporous IrO_2-400 samples.

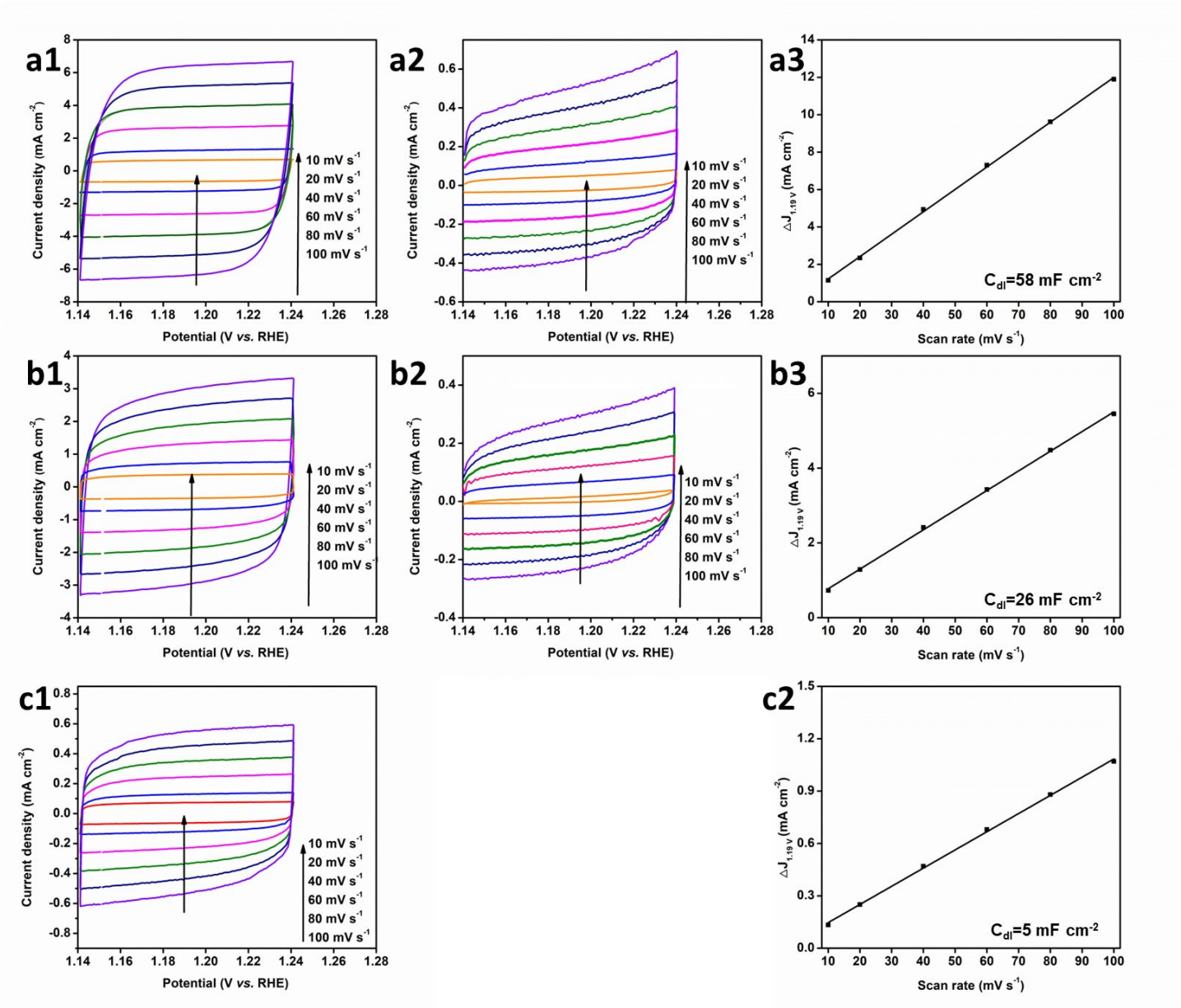

Figure S9 Cyclic voltammograms (CVs) of (a1) IrO_x-150 sample, (a2) pure carbon black and (a3) linear slope plotted from the CVs for the IrO_x-150 sample after subtraction of carbon black in 0.5 M H_2SO_4. Cyclic voltammograms (CVs) of (b1) IrO_2-400 sample, (b2) pure carbon black, and (b3) linear slope plotted from the CVs for the IrO_2-400 sample after subtraction of carbon black in 0.5 M H_2SO_4. Cyclic voltammograms (CVs) of (c1) commercial IrO_2 sample and (c2) linear slope plotted from the CVs for the commercial IrO_2 sample after subtraction of carbon black in 0.5 M H_2SO_4. The linear slopes are equivalent to twice the double-layer capacitance (C_{dl}).

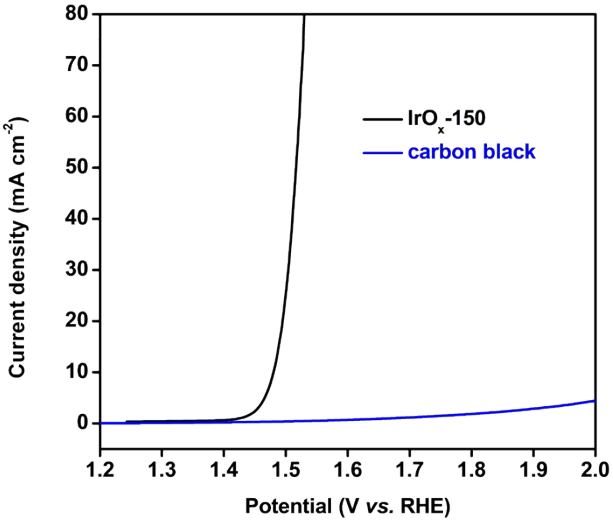

Figure S10 Polarization curves for mesoporous IrO_x-150 samples and carbon black measuring in 0.5 M H_2SO_4 solution at the scan rate of 5 mV s^{-1}.

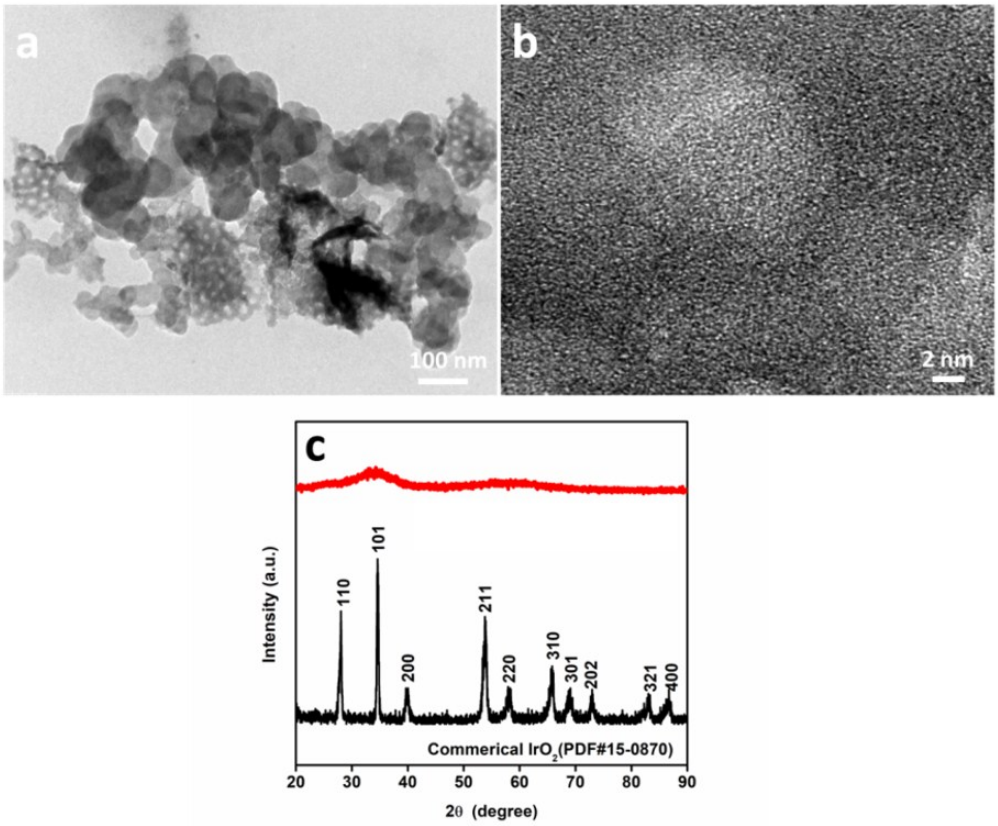

Figure S11 (a, b) TEM images and of the carbon-supported IrO_x-150 after testing. (c) Wide-angle XRD pattern of the same sample after testing.

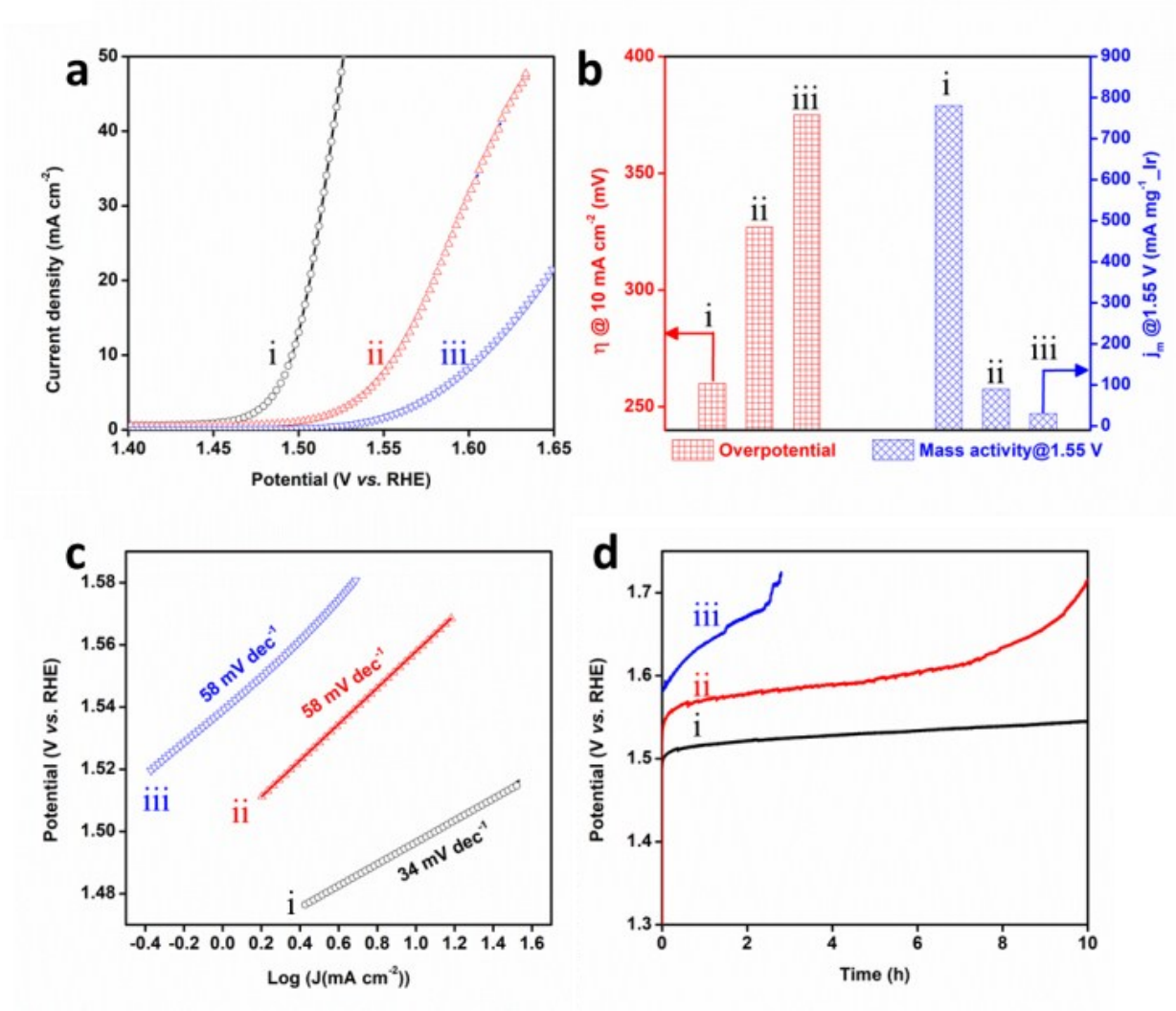

Figure S12 (a) Polarization curves for (i) mesoporous IrO_x-150, (ii) IrO_2-400 and (iii) commercial IrO_2 samples using 1 M KOH as the electrolyte at the scan rate of 5 mV s^{-1}. (b) Bar graph showing the overpotential (η_{10}) to drive 10 mA cm^{-2} and iridium mass activity (j_m) at 1.55 V (*vs*. RHE). (c) Tafel plots. (d) Chronopotentiometry curves of the catalysts at a constant current density of 10 mA cm^{-2}.

Table S2. Comparsion of the activity of mesoporous Ir nanosheets with previously reported Ir-based catalysts measured in acidic solution.

Sample name	Electrolyte	Tafel slope (mV dec^{-1})	η_{10} at corresponding j (mV)	Refrence
Mesoporous IrO_x-150 nanosheets	**0.5 M H_2SO_4**	**47 mV dec^{-1}**	**250 mV**	**Present work**
IrCoNi nanoframe	0.5 M H_2SO_4	54 mV dec^{-1}	303 mV	*Adv. Mater.* 2017, 29, 1703798
Ir anoparticles/graphene	0.5 M H_2SO_4	46 mV dec^{-1}	290 mV	*Nano Energy,* 2017, 40 27
$IrO_x/SrIrO_3$	0.5 M H_2SO_4	N/A	270 mV	*Science* 2016,353, 1011
IrO_x-Ir	0.5 M H_2SO_4	*ca.* 44 mV dec^{-1}	295 mV	*Angew. Chem., Int. Ed.* 2016, 55, 742
IrO_2/carbon nanotube	0.5 M H_2SO_4	67 mV dec^{-1}	293 mV	*ACS Catal*. 2017, 7, 5983
IrO_2-RuO_2@Ru	0.5 M H_2SO_4	53 mV dec^{-1}	281 mV	*J. Mater. Chem. A,* 2017, 5, 17221
Ir catalysts	1 M H_2SO_4	N/A	340 mV	*J. Am. Chem. Soc.* 2015, 137, 4347
Amorphous IrO_x film	1 M H_2SO_4	34 mV dec^{-1}	220 mV	*Chem. Mater.* 2014, 26, 1654
IrO_2 nanoneedle	1 M H_2SO_4	57 mV dec^{-1}	313 mV	*Adv. Funct. Mater.* 2018, 28, 1704796
$W_{0.57}Ir_{0.43}O_{3-\sigma}$	1 M H_2SO_4	85 mV dec^{-1}	370 mV	*Energy Environ. Sci.,* 2017, 10, 2432
IrNi oxide	0.1 M $HClO_4$	N/A	310 mV	*J. Am. Chem. Soc*. 2015, 137,13031
IrTe nanotubes	0.1 M $HClO_4$	60 mV dec^{-1}	290 mV	*J. Mater. Chem. A,* 2018, 6, 8855
IrO_2-TiO_2	0.1 M $HClO_4$	42 mV dec^{-1}	255 mV	*ACS Catal*. 2017, 7, 2346
Ba_2PrIrO_6	0.1 M $HClO_4$	54 ± 3 mV dec^{-1}	*ca.* 400 mV	*Nat. Commun.* 2016, 7, 12363
IrCu nanocage	0.1 M $HClO_4$	50 mV dec^{-1}	293 mv	*Adv. Funct. Mater.* 2017, 27, 1604688
3D Ir superstructure	0.1 M $HClO_4$	41 mV dec^{-1}	270 mV	*Nano Lett.* 2016,16, 4424
IrNiCu nanoframe	0.1 M $HClO_4$	48 mV dec^{-1}	300 mV	*ACS Nano* 2017, 11, 5500.
IrNi nanoparticles	0.1 M $HClO_4$	N/A	280 mV	*Adv. Funct. Mater.* 2017, 1700886
Mesoporous IrO_2 film	0.1 M $HClO_4$	N/A	270 mV	*Chem. Mater.* 2011, 23, 3201
$IrNiO_x$/Meso-ATO	0.05 M H_2SO_4	N/A	320 mV	*Angew. Chem. Int. Ed.* 2015,54, 2975